Superlattices and Microstructures 101 (2017) 261–270

Contents lists available at ScienceDirect

Superlattices and Microstructures

journal homepage: www.elsevier.com/locate/superlattices

Effect of nitrogen doping on the structural, optical and electrical properties of indium tin oxide films prepared by magnetron sputtering for gallium nitride light emitting diodes

Lifei Tian [a, b, **], Guoan Cheng [a, *], Hougong Wang [b], Yulong Wu [a], Ruiting Zheng [a], Peijun Ding [b]

[a] Key Laboratory of Beam Technology and Material Modification of Ministry of Education, College of Nuclear Science and Technology, Beijing Normal University, Beijing 100875, China
[b] Beijing North Microelectronics Company Limited, Beijing 100176, China

ARTICLE INFO

Article history:
Received 18 September 2016
Received in revised form 25 November 2016
Accepted 25 November 2016
Available online 28 November 2016

Keywords:
Indium tin oxide
Nitrogen doping
Magnetron sputtering
X-ray photoelectron spectroscopy
High resolution transmission electron microscope
Gallium nitride based light emitting diodes

ABSTRACT

The indium tin oxide (ITO) films are prepared by the direct current magnetron sputtering technology with an ITO target in a mixture of argon and nitrogen gas at room temperature. The blue transmittance at 455 nm rises from 63% to 83% after nitrogen doping. The resistivity of the ITO film reduces from 4.6×10^{-3} (undoped film) to 5.7×10^{-4} Ω cm (N-doped film). The X-ray photoelectron spectroscopy data imply that the binding energy of the $In3d_{5/2}$ peak is declined 0.05 eV after nitrogen doping. The high resolution transmission electron microscope images show that the nitrogen loss density of the GaN/ITO interface with N-doped ITO film is smaller than that of the GaN/ITO interface with undoped ITO film. The forward turn-on voltage of gallium nitride light emitting diode reduces by 0.5 V after nitrogen doping. The fabrication of the N-doped ITO film is conducive to modify the N component of the interface between GaN and ITO layer.

1. Introduction

Gallium nitride (GaN) based blue light emitting diodes play an important role in the applications of semiconductor lighting devices and liquid crystal displays [1–6]. A device of blue light emitting diode is usually constructed of sapphire substrate, GaN buffer layer, n-GaN layer, InGaN/GaN multiple quantum well layer, p-GaN layer and indium tin oxide (ITO) layer [7–9]. GaN is a kind of essential luminescence material in the device of blue light emitting diode [10–14]. ITO is a sort of significant transparent conductive oxide (TCO) material used in the device of blue light emitting diode [15–18], similar as zinc oxide material [19–21]. The ITO layer is usually fabricated by the sputtering technology [22–26].

One of the problems in the device of blue light emitting diode is that the light output efficiency is not high enough. There are two possible reasons for this problem according to the previous research [27–30]. One is that the optical and electrical

* Corresponding author.
** Corresponding author. Key Laboratory of Beam Technology and Material Modification of Ministry of Education, College of Nuclear Science and Technology, Beijing Normal University, Beijing 100875, China.
E-mail address: gacheng@bnu.edu.cn (G. Cheng).

http://dx.doi.org/10.1016/j.spmi.2016.11.054
0749-6036/

properties of the ITO layer are not enough, and another is that the interface structure between the p-GaN and the ITO layer are not perfect. The interface of ITO/p-GaN layer can be damaged during the deposition of ITO layer, resulting in the absence of nitrogen atoms in the surface of the p-GaN layer [31].

The ITO thin films with different nitrogen doping content (ITON) have different structures, resistivities and blue transmittances. It affects the light output efficiencies of GaN light emitting diodes by adopting the ITO thin films with different content of nitrogen. The use of the nitrogen doped ITO films in GaN light emitting diodes can improve the surface structure of GaN materials, and reduces the interface contact barrier of ITO/p-GaN layer and the turn on voltage of GaN light emitting diodes. Some previous studies have shown that the ITO film doesn't form ohmic contacts but the ITON film forms an ohmic contact after annealing on p-GaN layer [32]. However, nearly all the previous studies have shown that the resistivity of the ITO film increase after nitrogen doping in the radio frequency sputtering process [33–35].

In order to reduce the resistivity of the ITO film, the nitrogen doped ITO films fabricated on the c-plane sapphire substrate are investigated by using of nitrogen gas and direct current sputtering technology. Furthermore, the effect and mechanism of nitrogen doping on the optical and electrical properties, structures, component and surface morphology of the ITO films are discussed systematically. The nitrogen doped ITO layers with excellent performances are obtained, and have a potential application in the GaN based light emitting diode devices.

2. Experimental

The ITO thin film was deposited on the c-plane sapphire and GaN substrate by using of the direct current magnetron sputtering method. The nitrogen gas flows were 0, 1, 3, 4 and 5 sccm, respectively. The weight composition of the ITO target was 90%In_2O_3 and 10%SnO_2. The substrate temperature was at room temperature. The power of direct current was 200 W. The argon (Ar) gas flow was 80 sccm. The deposition time was 340 s and the thickness of the ITO thin film was 100 nm, which was measured by using of thin film thickness measuring instrument (Filmetrics F60-t).

The optical properties of the ITO films were measured by using of the ultraviolet-visible spectrophotometer (Shimadzu UV2450). The electrical properties were determined by using of the four point probe measuring instrument (CDE ResMap273). The structures of the ITO films were analyzed by X-ray diffractometer (XRD, PANalytical X′ Pert PRO MPD) with Cu K_α radiation and power source (40 kV, 40 mA). The surface morphology of the ITO films were analyzed by scanning electron microscopy (SEM, Hitachi SU8010) and atomic force microscopy (AFM, Vecco Dimension Edge), respectively. Three-dimension images were gained with scanning area 1 μm × 1 μm by AFM. The components of the ITO films were determined by X-ray photoelectron spectroscopy (XPS, Thermofisher ESCALAB 250Xi) with Al K_α radiation (1486.6 eV, monochromatized) and calibration using C1s line (284.8 eV). The nitrogen doping mechanism was analyzed by XPS valence band spectra and high resolution transmission electron microscope (HRTEM, FEI Tecnai G2 F20). The cross section images of GaN/ITO interface were determined by HRTEM in order to observe the nitrogen vacancies.

3. Results and discussion

3.1. Optical properties

The blue transmittance of the ITO film is one of the most important properties in the blue light emitting diode. Fig. 1(a) shows the curve of the blue transmittance at 455 nm of the ITO thin films versus nitrogen gas flow. From Fig. 1(a) we can see that the blue transmittance rises from 63% to 83% with the increase of nitrogen gas flow from 0 to 5 sccm. When the nitrogen gas flow grows to 3 sccm, the blue transmittance reaches at the maximum saturation value, i.e. 83%, which is improved by 30% than that of the undoped ITO films. The blue transmittance doesn't obviously change when the nitrogen gas flow rises from 3 to 5 sccm.

We have calculated the optical energy band gap (E_g) of the ITO thin films fabricated with different nitrogen gas flows according to Taue equation [36].

$$(\alpha h\nu)^2 = A(h\nu - E_g)$$

where, α is the absorption coefficient, hν is the photon energy, A is constant. Fig. 1(c) shows the curves of $(\alpha h\nu)^2$ versus photon energy. The absorption edge of the ITO thin films shifts towards the higher photon energy with the increase of nitrogen gas flow. The optical energy band gap of the ITO thin films rises from 4.53 to 4.96 eV when the nitrogen gas flow increases from 0 to 5 sccm. It indicates that the optical energy band gap of the ITO thin film become wider when doping N atoms into the ITO thin film.

3.2. Electrical properties

The electrical property of the ITO film is one of the most important properties in the blue light emitting diode. Fig. 2(a) and (b) show the sheet resistance (Rs) and resistivity of the deposited ITO thin films, respectively. Both of the sheet resistance and resistivity are lessened with the increase of the nitrogen gas flow. The resistivity declines from 4.6×10^{-3} to 5.7×10^{-4} Ω cm

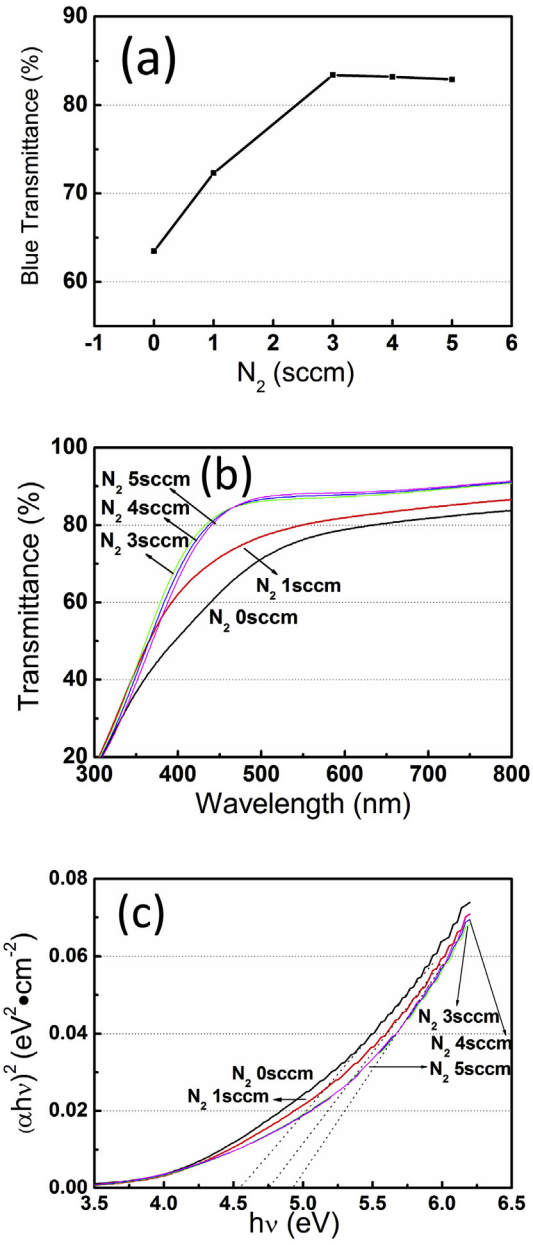

Fig. 1. Transmittances and absorbances of the ITO thin films fabricated with different nitrogen gas flows: (a) blue transmittance; (b) transmittance; (c) absorbance $((\alpha h\nu)^2$ versus photon energy).

while the nitrogen gas flow increases from 0 to 5 sccm. The electrical conductivity is enhanced by 80% through the nitrogen doping into the ITO thin films.

3.3. Structural properties

The optical and electrical properties of the ITO films exhibit great enhancements due to nitrogen doping into ITO films. In order to interpret these enhancements, the structures, component and surface morphology of the deposited ITO films are analyzed.

The XRD spectra of the ITO thin films fabricated with different nitrogen gas flows are shown in Fig. 3(a). From the XRD spectra of the ITO films, we can see that there are three crystal phases to be observed in the undoped ITO films, i.e. indium tin oxide ($In_4Sn_3O_{12}$), indium oxide (In_2O_3) and tin oxides (SnO_x). However, there are new crystal phases appearing in the N-doped ITO films, i.e. InN, Sn_xN_z and $Al_xO_{4-z}N_2$. The crystal phases of InN and Sn_xN_z indicate that the N

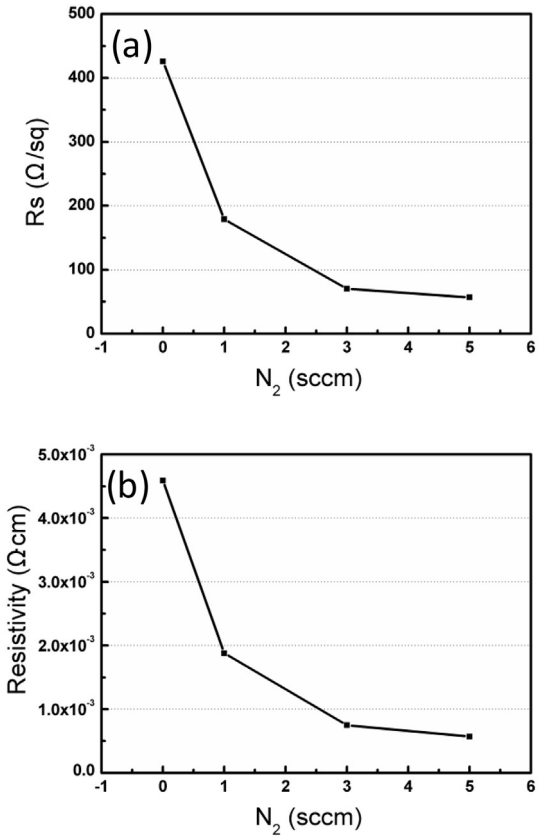

Fig. 2. Electrical properties of the ITO thin films fabricated with different nitrogen gas flows: (a) Rs, the sheet resistance; (b) resistivity.

atoms have been doped into the crystal structures of the ITO thin films. The crystal phase of $Al_xO_{4-z}N_2$ may come from the reaction of nitrogen gas (N_2) and sapphire substrate (Al_2O_3). It illuminates that the fabrication of the N-doped ITO film is conducive to modify the N component of the interface between the ITO layer and the substrate (including p-GaN layer).

The XRD spectra indicate that the ITO thin film is still polycrystalline after nitrogen doping. The crystal structure of the main phase $In_4Sn_3O_{12}$ belongs to the crystal system of hexagonal (JCPDS Card No. 88-0773). The 2θ of the main peak corresponding to $In_4Sn_3O_{12}(13\bar{2})$ enlarges 0.016°after adding the nitrogen gas to 5 sccm. That means the interplanar spacing of $In_4Sn_3O_{12}(13\bar{2})$ reduces after nitrogen doping according to the Bragg equation as following:

$$2d_{hkl}\sin\theta = \lambda,$$

where, d_{hkl} is the interplanar spacing of $In_4Sn_3O_{12}(13\bar{2})$, and λ is the wavelength of X-ray (0.154056 nm). Fig. 3(b) shows that the interplanar spacing of $In_4Sn_3O_{12}(13\bar{2})$ reduces from 0.20116 to 0.20109 nm after nitrogen doping. It indicates that the crystal lattice constant (a or c) of the $In_4Sn_3O_{12}$ phase becomes smaller due to nitrogen doping. The decrease of the crystal lattice constant of N-doped $In_4Sn_3O_{12}$ phase makes the optical energy band gap widen. The similar results have been reported in Ref. [33] where the wider band gap is related to structural changes. But there is a different result in the previous study [34] where the interplanar spacing of the main phase in the ITO film rises when adding the nitrogen gas to 50%. That may be ascribed to the different content of nitrogen gas.

The average grain size (L) of the phase $In_4Sn_3O_{12}$ is calculated through the Scherrer formula as following:

$$L = 0.89\lambda/\beta\cos\theta,$$

where, β is a full width at the half maximum of the main peak. Fig. 3(c) shows that the average grain size in the ITO thin film reduces from 3.6 to 2.4 nm after adding the nitrogen gas to 5 sccm. The decrease of the crystal lattice constant and average grain size indicate that the density of the ITO film is heightened due to the doping of nitrogen atoms, which can lead to the enhancement of the blue transmittance (as shown in Fig. 1(a)).

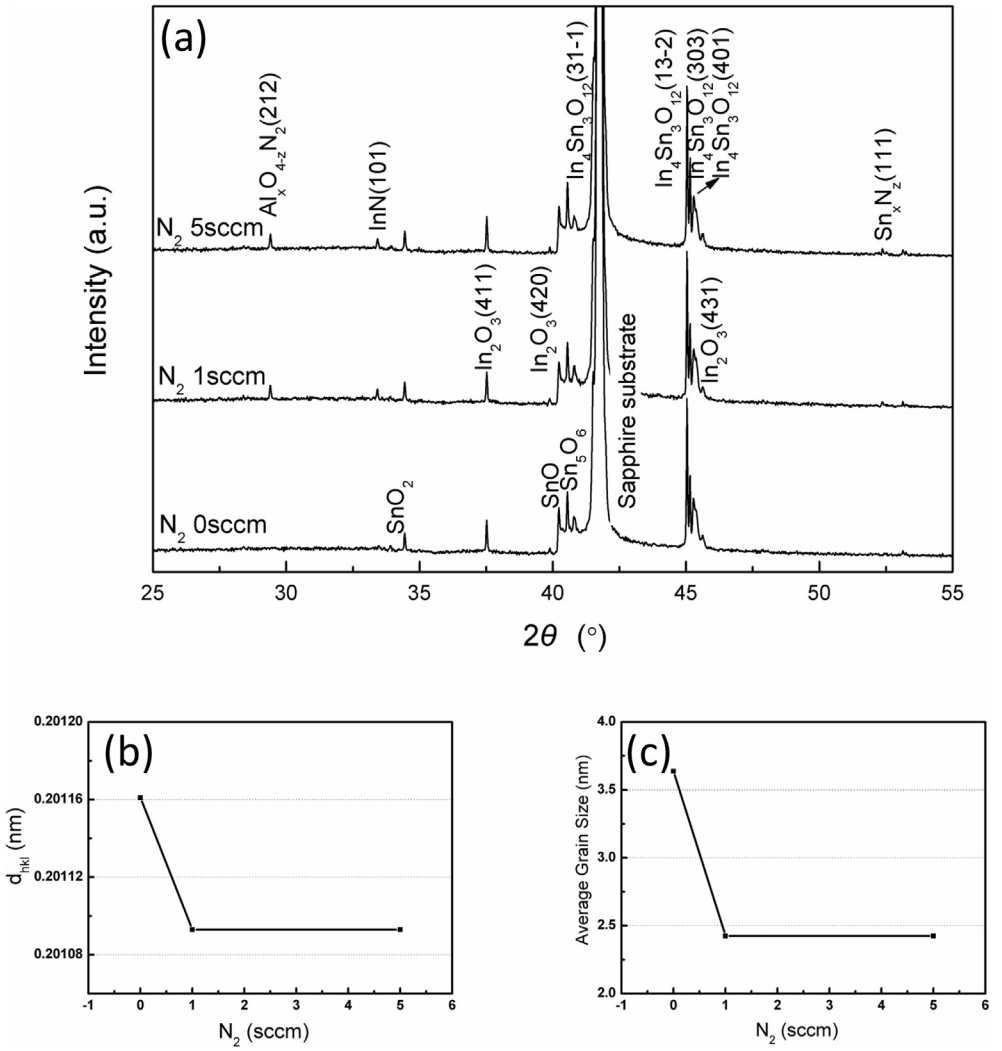

Fig. 3. XRD data of the ITO thin films fabricated with different nitrogen gas flows: (a) XRD patterns; (b) d_{hkl}, the interplanar spacing of $In_4Sn_3O_{12}(13\bar{2})$; (c) average grain size of $In_4Sn_3O_{12}$ phase.

3.4. Component of elements

The component in the ITO thin film is determined by XPS, as shown in Fig. 4. The element components in the ITO thin films fabricated with different nitrogen gas flows are shown in Fig. 4(a). The peaks of N1s, In3d, Sn3d and O1s are obtained and analyzed. The atomic concentrations of the four elements are calculated through the XPS spectra. The atomic concentrations of In and Sn have few changes when increasing the nitrogen gas flow. The atomic concentrations of N and O vary evidently with the increase of nitrogen gas flow. The atomic concentration of N rises and the atomic concentration of O declines after nitrogen doping. Fig. 4(b) shows the atomic concentration ratios of N and O in the ITO thin films fabricated with different nitrogen gas flows. The ratio of N and O (N/O) grows from 0 to 0.072 when the nitrogen gas flow increases from 0 to 5 sccm. The nitrogen doping atomic concentration in the ITO film rises from 0 to 3.4% after nitrogen doping. It suggests that the N can be doped into the ITO film by adding nitrogen gas during the sputter process.

Fig. 4(c) shows the XPS spectra of N1s core level. There is only one peak at the binding energy of 399.88 eV when the nitrogen gas flow is 0 sccm. This peak is ascribed to the N–O bonds located on the surface of the ITO thin film. These N–O bonds are formed by surface adsorption of the ITO film under ambient atmosphere. It is similar with the previous studies [32,37] where the N–O peak is at the binding energy of 400.0 eV. The intensity of this peak has a slight declination when the nitrogen gas flow increases from 0 to 5 sccm. It indicates that the surface adsorption concentration of N–O bonds declines after the nitrogen is doped into the ITO film, as shown in Fig. 4(d)i.

A new peak at the binding energy of 396.03 eV appears when introducing the nitrogen gas. This peak is ascribed to the N–In and N–Sn bonds in the ITO film. It is in agreement with previous studies [32,38]. The intensity of this peak is enhanced

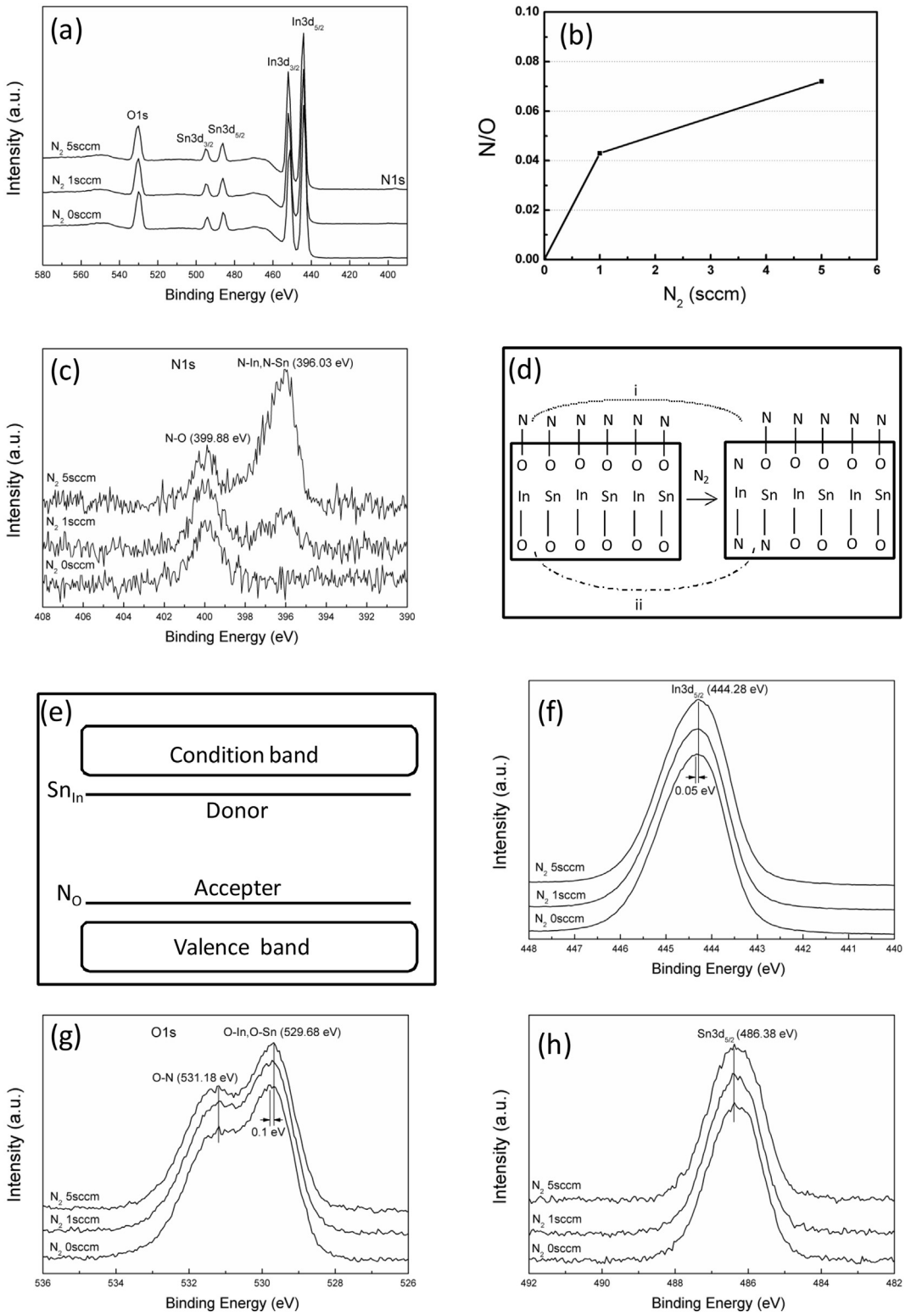

Fig. 4. Element components of the ITO films fabricated with different nitrogen gas flows: (a) XPS spectra; (b) N/O ratio; (c) XPS spectra of N1s; (d) diagrammatic sketch of substitution of N for O atoms; (e) diagrammatic sketch of energy level band in N-doped ITO thin films; (f) XPS spectra of $In3d_{5/2}$; (g) XPS spectra of O1s; (h) XPS spectra of $Sn3d_{5/2}$.

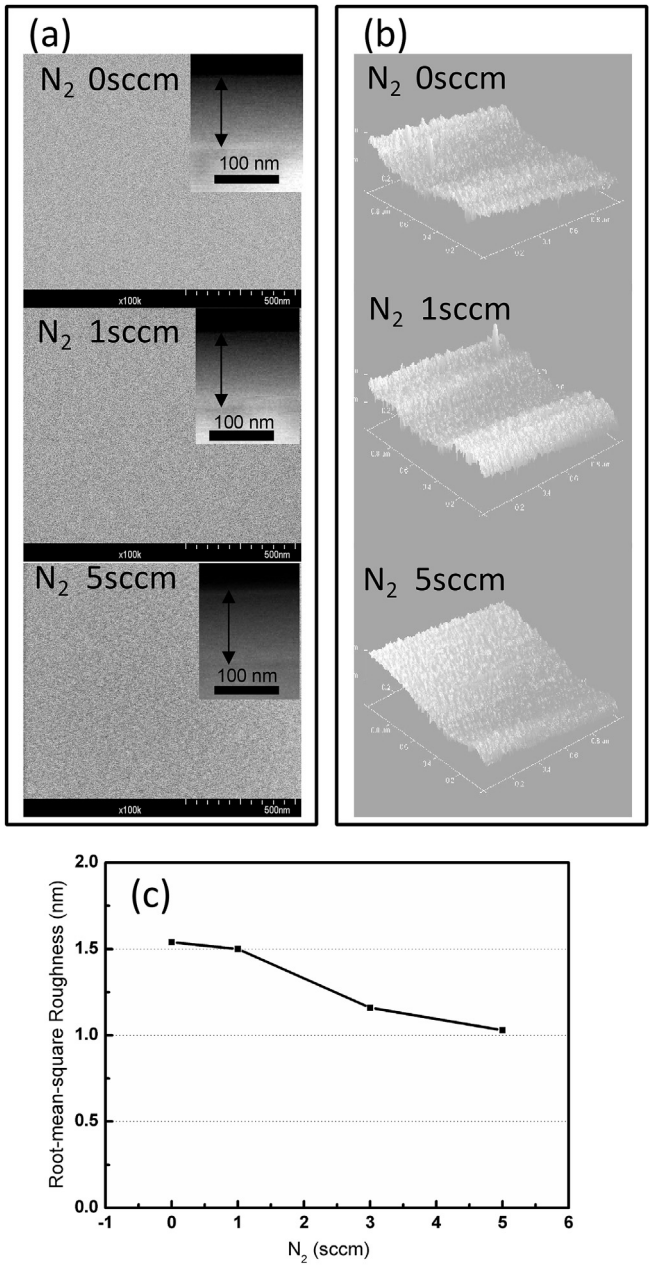

Fig. 5. Surface morphologies of the ITO films fabricated with different nitrogen gas flows: (a) top-view SEM images and inset is the cross section image; (b) three-dimension AFM images; (c) root-mean-square roughnesses.

prominently when the nitrogen gas flow increases from 0 to 5 sccm. It implies that the N atoms substitute partial O atoms and form the nitrogen-metal bonds (N–In, N–Sn), as shown in Fig. 4(d)ii. It is consistent with the XRD patterns shown in Fig. 3(a) where the new crystal phases InN and Sn_xN_z appears in the N-doped ITO films.

There are some O vacancies in the ITO films [39–41]. The occupancy of N for O vacancy and the substitution of N for O atom can introduce the impurity energy level of N_O which is near to the top of the valence band. The impurity energy level of N_O is an accepter level, while the impurity energy level of Sn_{In} is a donor level (as seen in Fig. 4(e)). The accepter levels may counteract all the donor levels so that the carrier concentration increases. The decrease of resistivity may result from the increase of the carrier concentration.

Fig. 4(f) shows the XPS spectra of $In3d_{5/2}$ core level in the ITO films fabricated with different nitrogen gas flows. The $In3d_{5/2}$ peak of the ITO film fabricated with nitrogen gas 5 sccm is at the binding energy of 444.28 eV corresponding to the O–In bonds [32]. The binding energy of $In3d_{5/2}$ peak is declined 0.05 eV when the nitrogen gas increases from 0 to 5 sccm. This is

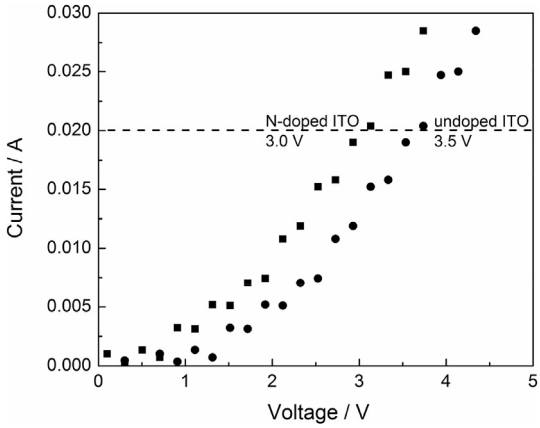

Fig. 6. The current-voltage curves of GaN-based LEDs fabricated with N-doped ITO and undoped ITO films.

resulted from the substitution of N—In for O—In bonds. The electro-negativity of N is weaker than O atom, so the binding energy of N—In is smaller than that of O—In bond. Therefore, the binding energy of the $In3d_{5/2}$ peak becomes smaller after the N—In bonds substitute part of the O—In bonds.

Fig. 4(g) shows the XPS spectra of O1s core level in the ITO films fabricated with different nitrogen gas flows. The main O1s peak of the ITO film fabricated with nitrogen gas 5 sccm is at the binding energy of 529.68 eV corresponding to O—In and O—Sn bonds [32,35]. The binding energy of the main O1s peak reduces 0.1 eV when the nitrogen gas flow increases from 0 to 5 sccm. Its shift is mainly resulted from partial substitutions of N—In for O—In bonds, and is similar to the $In3d_{5/2}$ peak. The secondary peak at the binding energy of 531.18 eV is related with some adsorbates (oxygen or water vapor) according to reference [42]. We ascribe this peak to N—O bonds located on the surface of the ITO film. It is identical to the N—O bonds in the XPS spectra of N1s. This peak has no shifts when increasing the nitrogen gas flow, and is similar to the $Sn3d_{5/2}$ peak at 486.38 eV [32] as shown in Fig. 4(h). That can be due to the stability of small Sn atomic content, 2.5% in the ITO thin films according to the calculation of XPS spectra.

3.5. Surface morphologies

The surface morphologies of the ITO thin films fabricated with different nitrogen gas flows are shown in Fig. 5. From the top-view SEM images in Fig. 5(a), we can see that the surfaces of the undoped and N-doped ITO thin films are all smooth and homogeneous. The sizes of grains on the surface of the ITO films are nearly the same when the nitrogen gas flow increases from 0 to 5 sccm. The insets of Fig. 5(a) show the cross section images of the ITO thin films fabricated with different nitrogen gas flows. It shows the cross section images of the ITO thin films are nearly the same.

Fig. 5(b) shows the three-dimension AFM images of the ITO thin films fabricated with different nitrogen gas flows. It indicates that the surface roughness of the ITO thin films is declined slightly after nitrogen doping. Fig. 5(c) shows that the surface root-mean-square roughness declines from 1.5 to 1.0 nm when the nitrogen gas flow increases from 0 to 5 sccm. It indicates that the surface of the ITO film becomes smoother after the N atom doping [35]. This is consistent with the XRD results shown in Fig. 3(c) where the average grain size of the ITO film reduces from 3.6 to 2.4 nm. The declination of the ITO surface roughness can lead to the decrease of resistivity shown in Fig. 2(b).

3.6. Performance of LED

Fig. 6 shows the curves of current versus voltage for GaN-based LEDs fabricated with N-doped ITO and undoped ITO films. From Fig. 6 we can see that, the forward turn-on voltages (corresponding to the current 20 mA) of LED fabricated with N-doped ITO and undoped ITO films are 3.0 and 3.5 V, respectively. The forward turn-on voltage reduces by 0.5 V after nitrogen doping. It can be concluded that the technology of doping nitrogen into ITO film is useful to reduce the forward turn-on voltage and improve the performance of GaN-based LEDs. It can modify the GaN/ITO interface by compensating for the nitrogen loss of the GaN surface.

3.7. The mechanism of nitrogen doping

The mechanism of nitrogen doping is investigated by XPS valence band spectra and high resolution TEM. Fig. 7 shows the XPS valence band spectra of the ITO thin films fabricated with different nitrogen gas flows. Two peaks at the binding energy of 4.27 and 7.67 eV are observed, respectively. The peak at 4.27 eV may be attributed to the In5p-O2p interaction and correspond to the p-like valence band orbital state, similar with InN [43]. The peak at 7.67 eV may be due to the In5s-O2p interaction and

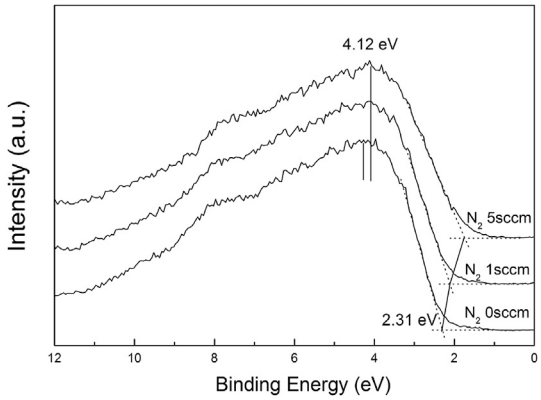

Fig. 7. XPS valence band spectra of the ITO thin films fabricated with different nitrogen gas flows.

correspond to the s-like valence band orbital state, similar with InN [43]. The peak at 4.27 eV shifts to 4.12 eV after nitrogen doping. The peak of InN is at the binding energy 3.5 eV [43], smaller than 4.27 eV of ITO. It can be deduced that the nitrogen atoms are doped into the ITO film and substitute partial oxygen atoms. The valence band maximum energy of ITO film declines from 2.31 to 1.74 eV when the nitrogen gas flow increases from 0 to 5 sccm. It means that the Fermi energy level of N-doped ITO film is closer to the valence band maximum than that of undoped ITO film. The N_O impurity level compensates partial Sn_{In} level so that the Fermi energy level shifts closer to the valence band maximum after nitrogen doping.

Fig. 8 shows the high resolution TEM images of the GaN/ITO interface with N-doped and undoped ITO films. The bigger white ball that is pointed by arrow on the GaN surface in Fig. 8 represent the nitrogen atom is lost. From Fig. 8 we can see that the nitrogen loss density of the GaN/ITO interface with N-doped ITO film is smaller than that of the GaN/ITO interface with undoped ITO film. The insets of Fig. 8 show the selected area diffraction images of the GaN/ITO interface. The main crystal planes of GaN are nearly the same, and the total number of crystal planes of the GaN/ITO interface with N-doped ITO film is bigger than that of the GaN/ITO interface with undoped ITO film. The crystal structure models of GaN are shown in the insets of Fig. 8. The black balls represent Ga atoms, and the white balls represent N atoms.

4. Conclusions

The N-doped ITO films have been prepared by using of the direct current magnetron sputtering technology. The N atoms doping into the ITO films improves the optical and electrical properties of the ITO films. The blue transmittance at 455 nm of the N-doped ITO film is improved by 30% than that of the undoped ITO film. The enhancement of blue transmittance is ascribed to the heightened ITO density. The decrease of the crystal lattice constant of the N-doped $In_4Sn_3O_{12}$ phase makes the optical energy band gap widen. The resistivity of the ITO film reduces from 4.6×10^{-3} (undoped film) to $5.7 \times 10^{-4}\ \Omega$ cm (N-

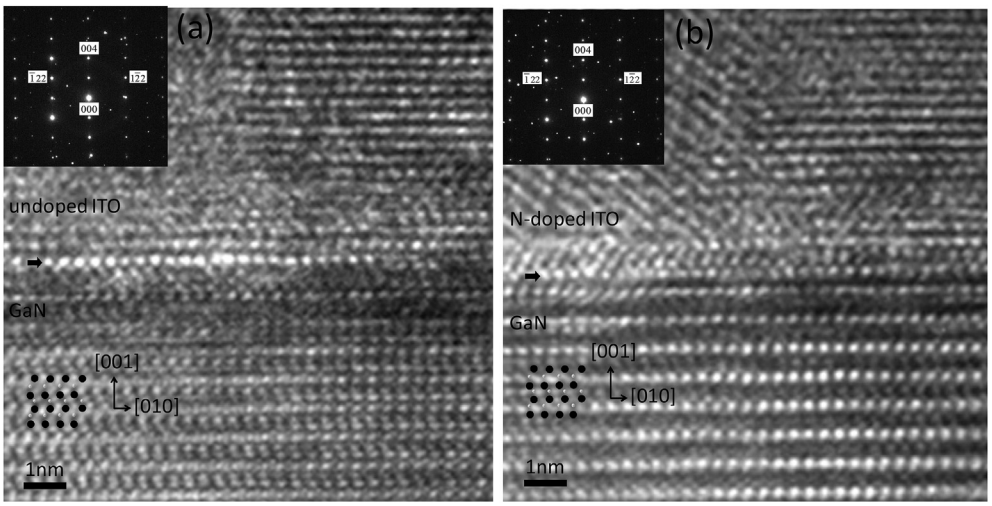

Fig. 8. High resolution TEM images of the GaN/ITO interface with N-doped and undoped ITO films. Insets: selected area diffraction spectra and crystal structure models (black ball represents Ga, white ball represents N).

doped film). The electrical conductivity of the ITO film is enhanced by 80% due to the carrier mobility increase through introducing the accepter impurity energy level of N_O. The surface of the N-doped ITO film becomes smoother than that of the undoped ITO film. The valence band maximum energy of ITO film declines from 2.31 to 1.74 eV when the nitrogen gas flow increases from 0 to 5 sccm. The high resolution transmission electron microscope images show that the nitrogen loss density of the GaN/ITO interface with N-doped ITO film is smaller than that of the GaN/ITO interface with undoped ITO film. The forward turn-on voltage of gallium nitride light emitting diode reduces by 0.5 V after doping nitrogen into the ITO film. The fabrication of the N-doped ITO film is conducive to modify the N component of the interface between p-GaN and ITO layer. These results illuminate that the N-doped ITO thin films will solve the problem of lower light output efficiencies of GaN light emitting diodes and have a potential application on GaN based blue light emitting diode devices in the future.

Acknowledgements

This work was supported by the National Basic Research Program of China (grant number 2010CB832905); the Program for New Century Excellent Talents in University (grant number NCET-11-0043); and the Fundamental Research Funds for the Central Universities.

References

[1] H. Masui, H. Yamada, K. Iso, J.S. Speck, S. Nakamura, S.P. Denbaars, J. Soc. Inf. Disp. 16 (2008) 571–578.
[2] Y.J. Lee, T.C. Hsu, H.C. Kuo, S.C. Wang, Y.L. Yang, S.N. Yen, Y.T. Chu, Y.J. Shen, M.H. Hsieh, M.J. Jou, Mater. Sci. Eng. B 122 (2005) 184–187.
[3] L.C. Chen, C.H. Tien, X. Liu, B. Xu, J. Nanomater. 2012 (2012) 5451–5463.
[4] K.J. Byeon, E.J. Hong, H. Park, J.Y. Cho, S.H. Lee, J. Jhin, J.H. Baek, H. Lee, Thin Solid Films 519 (2011) 2241–2246.
[5] J.C. Lee, Y.F. Wu, Thin Solid Films 518 (2010) 7437–7440.
[6] Z.C. Feng, L.H. Zhu, T.W. Kuo, C.Y. Wu, H.L. Tsai, B.L. Liu, J.R. Yang, Thin Solid Films 529 (2013) 269–274.
[7] K.J. Byeon, H. Park, J.Y. Cho, K.Y. Yang, J.H. Baek, G.Y. Jung, H. Lee, Phys. Status Solidi A 208 (2011) 480–483.
[8] K.M. Chang, J.Y. Chu, C.C. Cheng, C.F. Chu, Phys. Status Solidi 2 (2005) 2920–2923.
[9] K. Wu, T.B. Wei, D. Lan, H.Y. Zheng, J.X. Wang, Y. Luo, J.M. Li, Chin. Phys. B 23 (2014) 566–569.
[10] K.J. Byeon, J.Y. Cho, H.B. Jo, H. Lee, Appl. Surf. Sci. 346 (2015) 354–360.
[11] W.Z. Tawfik, S.J. Bae, S.W. Ryu, T. Jeong, J.K. Lee, Opt. Mater. 38 (2014) 131–136.
[12] W.Z. Tawfik, J. Song, J.J. Lee, J.S. Ha, S.W. Ryu, H.S. Choi, B. Ryu, J.K. Lee, Appl. Surf. Sci. 283 (2013) 727–731.
[13] P.C. Tsai, W.R. Chen, Y.K. Su, C.Y. Huang, Appl. Surf. Sci. 256 (2010) 6694–6698.
[14] B.H. Kong, W.S. Han, Y.Y. Kim, H.K. Cho, J.H. Kim, Appl. Surf. Sci. 256 (2010) 4972–4976.
[15] F. Jiang, J. Liu, L. Wang, C. Xiong, W. Fang, C. Mo, Y. Tang, G. Wang, L. Xu, J. Ding, X. Wang, Z. Quan, J. Zhang, M. Zhang, S. Pan, C. Zheng, Sci. Sin. Phys. Mech. Astron 45 (2015) 067302.
[16] F. Rao, X. Zhu, A. Xu, J. Chu, Y. Zhang, Acta Opt. Sin. 35 (2015) 0130002.
[17] H.G. Hong, S.S. Kim, D.Y. Kim, T. Lee, J. Song, J.H. Cho, C. Sone, Y. Park, T.Y. Seong, Appl. Phys. Lett. 88 (2006) 103505.
[18] H. Chun, P. Manousiadis, S. Rajbhandari, D.A. Vithanage, IEEE Photonic. Tech. L. 26 (2014) 2035–2038.
[19] J.W. Wang, J.M. Bian, J.C. Sun, H.W. Liang, J.Z. Zhao, G.T. Du, Acta Phys. Sin. – Ch. Ed. 57 (2008) 5212–5216.
[20] Y.J. Zhao, D.Y. Jiang, M. Zhao, R. Deng, J.M. Qin, S. Gao, Q.C. Liang, J.X. Zhao, Appl. Surf. Sci. 266 (2013) 440–444.
[21] P. Cao, D.X. Zhao, D.Z. Shen, J.Y. Zhang, Z.Z. Zhang, Y. Bai, Appl. Surf. Sci. 255 (2009) 3639–3641.
[22] K.C. Heo, Y. Sohn, J.S. Gwag, Ceram. Int. 41 (2015) 617–621.
[23] C. Huang, Y. Li, Y. Zhang, M. Wang, Y. Zhang, Z. Jia, J. Synth. Cryst. 44 (2015) 1051–1055.
[24] C.L. Liang, G.A. Cheng, R.T. Zheng, H.P. Liu, J.C. Li, H.F. Zhang, G.J. Ma, Y.L. Jiang, Surf. Coat. Tech. 201 (2006) 5537–5540.
[25] J.H. Deng, R.T. Zheng, Y. Zhao, G.A. Cheng, ACS Nano 6 (2012) 3727–3733.
[26] J.H. Deng, R.T. Zheng, Y.M. Yang, Y. Zhao, G.A. Cheng, Carbon 50 (2012) 4732–4737.
[27] Y. Cheng, T. Zhan, J. Ma, L. Zhang, Z. Si, X.Y. Yi, G.H. Wang, J.M. Li, Mater. Sci. Semicond. Process 17 (2014) 100–103.
[28] G. Halpin, T. Robinson, X.M. Jin, X.N. Kang, G.Y. Zhang, IEEE Photonics J. 6 (2014) 1–10.
[29] Y. Kashiwagi, A. Koizumi, Y. Takemura, S. Furuta, M. Yamamoto, M. Saitoh, M. Takahashi, T. Ohno, Y. Fujiwara, K. Murahashi, K. Ohtsuka, M. Nakamoto, Appl. Phys. Lett. 105 (2014) 223509.
[30] W.C. Lai, C.N. Lin, Y.C. Lai, P.C. Yu, G.C. Chi, S.J. Chang, Opt. Express 22 (2014) A396–A401.
[31] S.J. Chang, C.H. Lan, J.D. Hwang, Y.C. Cheng, W.J. Lin, J.C. Lin, H.Z. Chen, J. Electrochem. Soc. 155 (2008) H140–H143.
[32] M. Himmerlich, M. Koufaki, G. Ecke, C. Mauder, V. Cimalla, J.A. Schaefer, A. Kondilis, N.T. Pelekanos, M. Modreanu, S. Krischok, E. Aperathitis, ACS Appl. Mater. Interfaces 1 (2009) 1451–1456.
[33] E. Aperathitis, M. Modreanu, M. Bender, V. Cimalla, G. Ecke, M. Androulidaki, N. Pelekanos, Thin Solid Films 450 (2004) 101–104.
[34] E. Aperathitis, M. Bender, V. Cimalla, G. Ecke, M. Modreanu, J. Appl. Phys. 94 (2003) 1258–1266.
[35] M. Gartner, H. Stroescu, A. Marin, P. Osiceanu, M. Anastasescu, M. Stoica, M. Nicolescu, M. Duta, S. Preda, E. Aperathitis, A. Pantazis, V. Kampylafka, M. Modreanu, M. Zaharescu, Appl. Surf. Sci. 313 (2014) 311–319.
[36] R. Chandra, A.K. Chawla, P. Ayyub, J. Nanosci. Nanotechnol. 6 (2006) 1119–1123.
[37] M. Himmerlich, M. Koufaki, C. Mauder, G. Ecke, V. Cimalla, J.A. Schaefer, E. Aperathitis, S. Krischok, Surf. Sci. 601 (2007) 4082–4086.
[38] Y. Inoue, M. Nomiya, O. Takai, Vacuum 51 (1998) 673–676.
[39] M. Koufaki, M. Sifakis, E. Iliopoulos, N. Pelekanos, M. Modreanu, V. Cimalla, G. Ecke, E. Aperathitis, Appl. Surf. Sci. 253 (2006) 405–408.
[40] T.S. Moss, P.W. Levy, Phys. Today 13 (1960) 56–58.
[41] L. Gupta, A. Mansingh, P.K. Srivastava, Thin Solid Films 176 (1989) 33–44.
[42] J.C.C. Fan, J.B. Goodenough, J. Appl. Phys. 48 (1977) 3524–3531.
[43] D. Skuridina, D.V. Dinh, B. Lacroix, P. Ruterana, M. Hoffmann, Z. Sitar, M. Pristovsek, M. Kneissl, P. Vogt, J. Appl. Phys. 114 (2013) 173503.